Comparison of silicon photonic crystal resonator designs for optical trapping of nanomaterials

2010 Nanotechnology 21 305202

(http://iopscience.iop.org/0957-4484/21/30/305202)

Nanotechnology **21** (2010) 305202 (8pp) doi:10.1088/0957-4484/21/30/305202

Comparison of silicon photonic crystal resonator designs for optical trapping of nanomaterials

X Serey[1], **S Mandal**[2] **and D Erickson**[2]

[1] School of Applied and Engineering Physics, Cornell University, Ithaca, NY 14850, USA
[2] Sibley School of Mechanical and Aerospace Engineering, Cornell University, Ithaca, NY 14850, USA

E-mail: de54@cornell.edu

Received 9 March 2010, in final form 4 June 2010
Published 6 July 2010
Online at stacks.iop.org/Nano/21/305202

Abstract

The use of silicon photonic devices for optical manipulation has recently enabled the direct handling of objects like nucleic acids and nanoparticles that are much smaller than could previously be trapped using traditional laser tweezers. The ability to manipulate even smaller matter however requires the development of photonic structures with even stronger trapping potentials. In this work we investigate theoretically several photonic crystal resonator designs and characterize the achievable trapping stiffness and trapping potential depth (sometimes referred to as the trapping stability). Two effects are shown to increase these trapping parameters: field enhancement in the resonator and strong field containment. We find trapping stiffness as high as 22.3 pN nm^{-1} for 100 nm polystyrene beads as well as potential depth of 51 000 $k_B T$ at $T = 300$ K, for one Watt of power input to the bus waveguide. Under the same conditions for 70 nm polystyrene beads, we find a stiffness of 69 pN nm^{-1} and a potential depth of 177 000 $k_B T$. Our calculations suggest that with input power of 10 mW we could trap particles as small as 7.7 nm diameter with a trapping depth of 500 $k_B T$. We expect these traps to eventually enable the manipulation of small matter such as single proteins, carbon nanotubes and metallic nanoparticles.

(Some figures in this article are in colour only in the electronic version)

1. Introduction

Since the original experiments reported in Ashkin's founding article [1], optical or laser tweezing techniques [2] have been used in a large number of different areas including: single cell dynamics [3], optical chromatography [4, 5], directed assembly [6, 7], and have already helped understand complex phenomena like cellular motility [8] and single DNA mechanical properties [9]. Though extremely successful at these size scales a limitation of traditional optical tweezers is in manipulating smaller dielectric objects, on the order of 100 nm or less. A few optical tweezing techniques have been developed to trap nanoscopic objects [10, 11] but not generally pure dielectrics which are closer approximations to biological species. From Rayleigh theory it is well known that the optical gradient force, which is usually exploited as the trapping force in optical tweezers, scales with the radius of the particle cubed [12]. Roughly speaking then, it takes a 1000 fold increase in the applied trapping power to apply the same force to a particle that is only ten times smaller.

In order to overcome this limitation a number of new, near field optical manipulation techniques have been developed which exploit the strong forces that can be generated in the near field of plasmonic or resonant photonic structures. These devices, recent variations of which include plasmonic tweezer [13–15], whispering gallery mode carousel [16] and photonic crystal resonators [17–19], have the added benefit of also being in a format which can be readily integrated with a lab-on-chip device while exploiting the enhanced field provided by photonic resonances. Further improvements in these devices have recently been introduced by allowing the full strength field directly interact with the trapped particle using either slot and hole apertures [17, 18, 20, 21]. Using the photonic crystal resonator, we have been able to evanescently

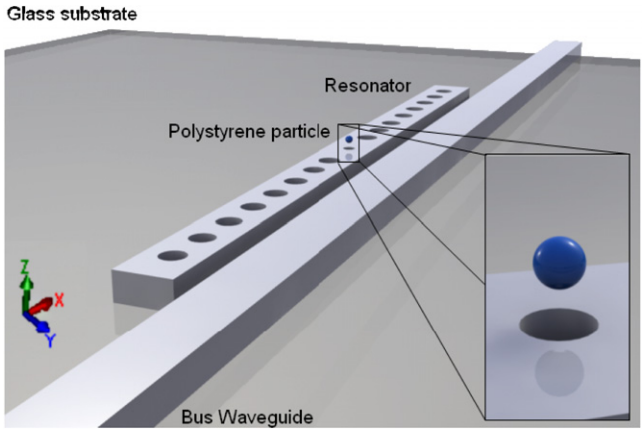

Figure 1. Evanescently coupled linear resonator for optical trapping. In this study we investigated three resonator designs including the 'microcavity plus hole' (MH) design shown here. The trapped particle is shown above the central hole.

trap particles as small as 48 nm in diameter [19]. The experimentally demonstrated state of the art technique in terms of high trapping stiffness is provided by the Self-Induced Back Action design trapping 50 nm particles with a stiffness of the order of 7 pN nm^{-1} W^{-1}.

With the aim of being able to optically manipulate even smaller material, we explore theoretically the trapping potential of a number of silicon photonic crystal resonator designs and evaluate them against techniques such as those described above. In the devices we examine here, the resonators are excited through evanescent coupling from a bus waveguide (figure 1) as this offers the greatest multiplexing possibilities and is in line with what we have demonstrated experimentally [22]. To the best of our knowledge it is the first time comprehensive calculations are performed with resonant devices to evaluate the trapping stiffness and stability. It is essential to perform comprehensive calculations since the Rayleigh approximation does not hold for the same range of particle sizes in tightly confined electromagnetic fields. The sizes of the particles considered in this work are in the limit of the Rayleigh approximation range. In our devices, the perturbative approach is also affected by the inaccuracy of the Clausius–Mossotti polarizability in fields with high gradients. In a previous work, Barth *et al* [17] performed exact calculation to estimate the dependence of resonant traps on the size of the trapped bead. Recently, Lin *et al* [18] performed perturbative calculations to estimate the trapping capacity. In this paper, we present an exact approach to the stiffness evaluation while addressing the issues arising from the resonant wavelength shift that Barth *et al* predicted by taking great care to distinguish the numerical impact and the physical contribution.

In the first two sections of this paper, we introduce the three devices we focused on, namely the microcavity design (MD), the mode gap design (MG), and the microcavity plus hole design (MH), and then the details of the numerical analysis method used to characterize them. After that we present and discuss the results in sections 4 and 5 focusing on the MH design because it offers the highest stiffness and stability. Tables in section 4 provide direct comparison of these results with the state of the art.

2. System description

Optical resonators are devices in which photons travel along a closed path. Fabry–Pérot resonators represent a class of resonator in which light bounces back and forth between two facing mirrors. In such a cavity, the allowed modes are those where the different light rays constructively interfere with each others. The resonant condition is given by the constructive interference condition that the phase delay in the resonator should be an integer multiple of 2π. In photonic crystal resonators, the cavity is sandwiched between two photonic crystal mirrors, thus presenting a newer version of the Fabry–Pérot resonator (figure 1). The sub-diffraction limited field confinement allows for higher gradients. According to the Rayleigh theory, the trapping force is proportional to the gradient of E^2 [12]. Hence we obtain higher forces with tighter field confinement. The stable position is located at the maximum of the field. In their movement, the particles will preferably follow the streamlines of the gradient of E^2 towards the stable position.

In figure 2, we present the three photonic crystal resonator designs examined here, which we refer to herein as: the microcavity design (MD), the mode gap design (MG), and the microcavity plus hole design (MH). All the resonator devices presented here were assumed to have the bulk properties of silicon (refractive index $n_{\text{silicon}} = 3.47$) and had cross-sectional dimensions of 250 nm high by 450 nm wide. As shown in figure 1, light was coupled into the resonators evanescently from another silicon bus waveguide (also 250 nm height per 450 nm large) which ran alongside the resonator. The devices lie on a silica substrate ($n_{\text{glass}} = 1.45$), mimicking a device fabricated from a silicon-on-insulator wafer, and the surrounding medium is assumed to be water ($n_{\text{water}} = 1.33$). The MD design (figure 2(a)) consists of two identical tapered Bragg mirrors [23]. Each reflector comprises of seven holes of radius 100 nm separated by a lattice constant $a = 390$ nm. An eighth hole at distance $0.9 * a$ is added and serves as a taper. The microcavity itself has a total length of $1.5 * a$. As in the MD device, the MH device is an implementation of Velha *et al*'s [23] design for high quality factor 1D photonic crystals. The MH device and the MD are very similar, with the difference being that an additional 50 nm radius hole is placed at the centre of the cavity region. It serves as an inner cavity in which light the intensity will be increased, the effect is clearly visible in figure 2(b), which is exposed to the liquid state for trapping. At any liquid/silicon boundary, the field is increased because of boundary conditions and then vanishes as an evanescent wave. The superposition of these evanescent waves in the inner cavity hole is what allows for the formation of this high field intensity region. The MG design is inspired from mode gap photonic crystal resonators, which have recently been demonstrated to exhibit very high quality factors. The MG design (figure 2(c)) consists of a standard periodic photonic crystal (same lattice constant a) where the radius of the etched holes varies from 100 nm at the edges to 40 nm at the centre.

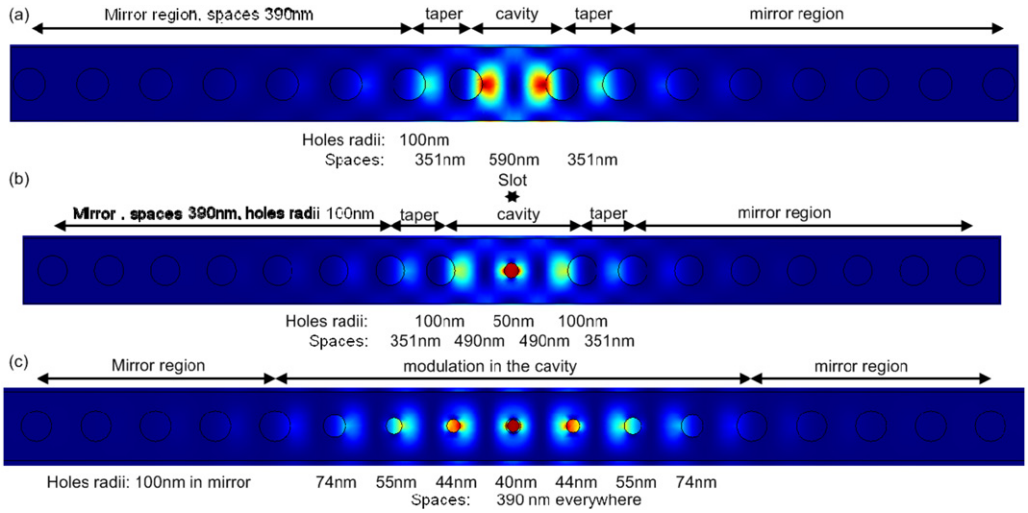

Figure 2. Specifications for the three photonic crystal resonator devices investigated here showing the computed electric field at resonance. (a) The Microcavity design, (b) the Microcavity plus Hole design, and (c) and the Mode Gap design. In all figures, the spaces refers to the centre-to-centre distance between the holes. The core photonic crystal was chosen such that it acts as a mirror for 1550 nm wavelength light.

3. Details of numerical analysis

The numerical technique we used here consisted of repeatedly computing the trapping forces while shifting the particle's physical position along one of the main axes (figure 1). The force was estimated through the Maxwell stress tensor [24] given a geometrical frame and its related refractive indices list. The simulations performed here were done using a commercial finite element code (COMSOL). The finite element method, FEM, was preferred over a finite difference time domain, FDTD, technique due to much lower time memory requirements. The long photon residence time in the high quality factor optical resonators necessarily results in an extremely long simulation time in order to accurately compute the fields and forces using an FDTD method. A drawback was that wavelength dependant estimations required several FEM simulations whereas one FDTD simulation would have sufficed. For the calculation of wavelength dependant quantities below, we parameterized the simulation and solved for wavelengths spanning the resonant domain. The Q factor is an example of a wavelength dependant quantity, which was approximated here via equation (1).

$$Q \approx \frac{\lambda_r}{\Delta\lambda}. \tag{1}$$

In this formula, knowledge of λ_r the resonant wavelength and of $\Delta\lambda$ the full width at half maximum is required.

The main objective of the simulations was to predict the trapping capabilities of the three designs discussed above. In all cases the trapping forces were computed by including a polystyrene bead ($n_{\text{polystyrene}} = 1.59$) in the computational domain and then integrating the Maxwell stress tensor over an artificial boundary region that included the particle.

$$\vec{F}_{\text{EM}} = \oint \overline{\overline{T}}_{\text{Maxwell}} \cdot \vec{n}\, \mathrm{d}S. \tag{2}$$

In this expression $\boldsymbol{F}_{\text{EM}}$ is the electromagnetic force, $\boldsymbol{T}_{\text{Maxwell}}$ is the Maxwell stress tensor and $\boldsymbol{n}$ is the outgoing vector normal to the surface. In our simulations, the integration surface was a sphere 10 nm bigger in radius than the particle itself. We verified that changing the integration surface did not affect significantly the computed force.

A number of mesh quality experiments were conducted in order to ensure convergence of the solution. Generally speaking, higher mesh qualities were required in the region of the particle and integrating sphere in order to obtain the expected resonance condition and convergence of the force value. We found that the simulation's meshing affected the numerical resonant wavelength. This alteration was not physical and was disregarded by ensuring the resonant condition in all simulations. For higher Q factors or larger particle sizes, the particle's position would have a sufficiently pronounced effect on the resonant wavelength that it could significantly alter the trapping conditions. We describe in the end of section 5 how, in cases where this resonance shift is important, this can become a practical advantage by making the wavelength a tuneable trapping element.

From the force calculations, we were able to extract two parameters commonly used to describe optical traps: the trapping stability [12] and the trapping stiffness [25]. To do this, we start the calculation from the stable position, which is the equilibrium point, and move the particle away from it repeating the force computation at every point. For distances not too far from the equilibrium point, the force response is similar to a linear spring where the spring constant is equal to the trapping stiffness. The trapping stiffness therefore, is the derivative of the restoring force with respect to the position perturbation around the equilibrium point as described by equation (3).

$$k_i = \left(\frac{\partial F_i}{\partial X_i}\right)_{\text{equilibrium}}. \tag{3}$$

Table 1. Calculated stiffness' for MD, MG and MH designs for 100 nm particle.

Resonator design	Microcavity design (MD)	Mode gap design (MG)	Microcavity plus hole (MH)
X-direction stiffness (pN nm^{-1} W^{-1})	4.81	13.1	22.3
Y-direction stiffness (pN nm^{-1} W^{-1})	3.30	14.0	37.5
Z-direction stiffness (pN nm^{-1} W^{-1})	8.53	31.3	65.5
Effective stiffness (pN nm^{-1} W^{-1})	3.30	13.1	22.3
Maximum force (pN W^{-1})	700	2070	4100
Q factor	500	1400	2200

Table 2. Comparison of stiffness' for several trapping devices recently published.

Device	Trapped particle, size (nm)	Trapping stiffness (pN nm^{-1} W^{-1})
Microcavity design (MD)	Polystyrene, 100	3.30
	Polystyrene, 200	7.93
Mode gap design (MG)	Polystyrene, 100	13.1
	Polystyrene, 200	26.85
Microcavity plus hole (MH)	Polystyrene, 100	22.3
Self-induced back action [21]	Polystyrene, 100	8.2
	Polystyrene, 50	6.6
Slot waveguides [20]	Polystyrene, 100	0.2
Plasmonic tweezer [14]	Polystyrene, 200	0.013
Conventional tweezer [28]	Polystyrene, 220	0.027
Standing Gaussian wave [29]	Polystyrene, 100	1

In this equation, k_i and F_i are the stiffness and force in the direction parameterized by X_i. These values are computed for 1 W of laser power into the bus waveguide, we use the units per Watt to lift this dependence as all of the numbers we present are proportional to the input power. The trapping stiffness can be evaluated along the three coordinate axes with the lowest result representing the limiting one. Hence we refer to it as the effective stiffness. The harmonic approximation also allows us to express the mean displacement of the particle when trapped in the potential. We can express the mean deviation $\langle x^2 \rangle$ using the equipartition theorem:

$$k\langle x^2 \rangle = k_B T \tag{4}$$

where k is the effective stiffness of the trap—i.e. the stiffness in the weakest direction—, x is the displacement along one direction, k_B is the Boltzmann constant and T is the temperature in kelvin.

The other parameter is of interest here is the trapping stability, which is related to the likelihood of the random thermal energy being able to free the particle from the trap. The stability leads to the average trapping time proportional to its exponential following a Kramers escape process [26]. It is defined as the ratio of the potential energy depth to the available thermal energy as shown in equation (5).

$$S = \frac{W}{k_B T}. \tag{5}$$

Here, W the work necessary to bring the particle from a free position to the stable point for 1 W of pumping power to the waveguide, k_B and T were already introduced in equation (4). The potential energy is equal to the opposite of the work necessary to bring the particle from a free position to the equilibrium trapped position. In accordance with analytical expectations [27], we used an exponential interpolation of the decaying force profile as the particle rises away from the resonator in the evanescent field to compute the release work W.

4. Results

4.1. Particles larger than the diameter of the central cavity hole

Using the simulation methods described above, we evaluated the trapping characteristics of the three designs. In table 1 we report the trapping stiffnesses along all three coordinate axes and maximum force, for the MD, MH and MG devices as described in section 2. As can be seen the MH design exhibited the highest stiffness and thus we will expand on that here as an illustrative case. Figure 3 illustrates the electric field and force profiles computed as described above. For a 100 nm particle, the trapping stiffnesses for the MH design were found to be 22.3 pN nm^{-1} W^{-1} and 37.5 pN nm^{-1} W^{-1} in the X and Y directions respectively. The X and Y stiffnesses were calculated for a particle which bottom was positioned 20 nm above the resonator surface with a 1 W of laser power input into the bus waveguide. The stable position of the MH resonator coincided with the centre of the device. The electric field is polarized in the Y direction; hence boundary discontinuity conditions induce a higher gradient along that axis accounting for the larger stiffness value. Along the Z-axis (figure 3(d)), an exponential decay in the force profile was obtained which is consistent with the evanescent nature of the field outside the resonator. The decay length, the inverse of the argument in the exponential, was 50 nm and the calculated stiffness was 65.5 pN nm^{-1} W^{-1}. Therefore the effective stiffness of the MH design is 22.3 pN nm^{-1} W^{-1}.

Stiffness' are the result of the linear interpolation of the F_{X_i} versus X_i curve around the equilibrium point of the device. When compared with the state of the art devices described in the introduction, the MH device yields stiffness' and stability values significantly higher than other tweezers. In table 2, we have tabulated reported stiffnesses from recently published articles and compared them to the results obtained here. The SIBA tweezer, which reports the highest published stiffness to date, offers a 8.2 pN nm^{-1} W^{-1} effective stiffness for 100 nm polystyrene ($n = 1.575$) [21]. It uses the optical resonance of a light wave propagating through a small aperture. When a particle is present in the aperture, it induces a shift in the resonance. By illuminating the aperture with a detuned wavelength, the particle induces the resonance. It is the fact that the resonance is sensitive in the position of the particle that allows such high stiffness. The maximum force remains of the order of 250 pN W^{-1} for a 100 nm particle [21]. The resonant nanotweezer described here can offer forces as high as 4.1 nN W^{-1}. This can be compared to the typical force exerted by the evanescent field of a waveguide which is of the order of 1 pN W^{-1}.

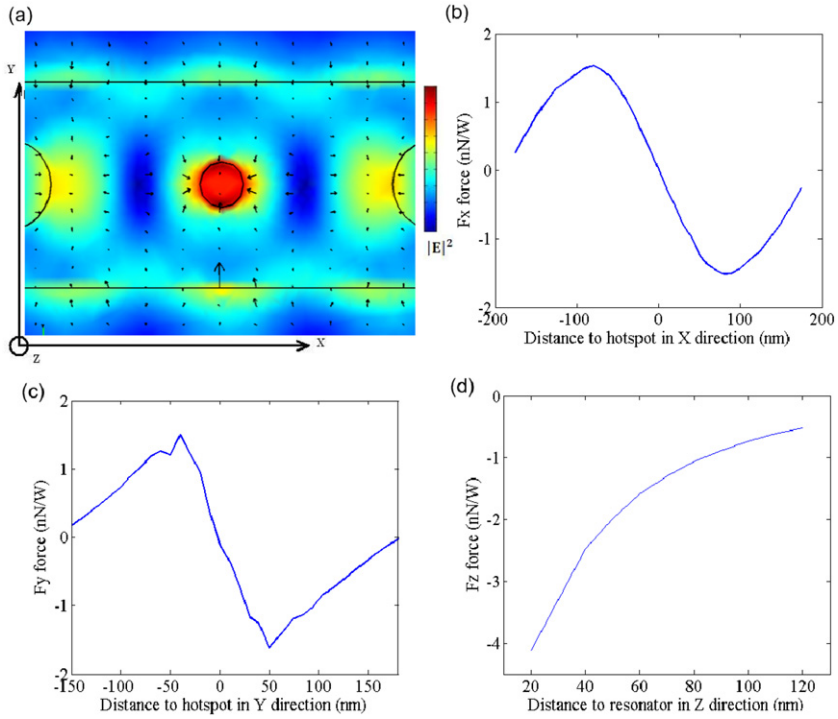

Figure 3. Numerical results for the microcavity plus hole (MH) device. (a) Field intensity and its gradient (arrow plot) when the MH trapping design is on resonance without a particle in the simulation domain. (b) and (c) Force profiles for the particle as it is moved along the resonator (X axis) and across the resonator (Y axis). In all simulations the particle was maintained at a vertical height of 20 nm above the resonator. (d) Z-axis force profile computed as the particle is maintained above the resonator's centre and moved from 20 nm to 120 nm above top plane of the device. The stiffnesses were evaluated using linear interpolation around the stable position. In the X and Y directions (b), (c) the linear approximation is very accurate. In the Z direction (c), we did not take the slope at $Z = 20$ nm but also linearly interpolated the data between 20 and 80 nm which is a conservative estimate. (b)–(d) All calculations done for a polystyrene bead ($n = 1.59$) with a diameter of 100 nm.

As alluded to above, the stability factor is the ratio of the work required to remove the particle from the trap, to the random thermal energy in the system. Very stable traps therefore have $S \gg 1$, and unstable traps have $S < 1$. We calculated the potential energy of the trap by integrating the work needed to release the particle from 20 nm above the resonator's centre to a distance far away from it such that the particle no longer feels the trapping force. In order to be consistent with the rest of the data, we have calculated the work to extract the particle from a position 20 nm above the resonator. The results for all three designs presented here are shown in table 3. As can be seen, the trapping stabilities as high as 44 000 W^{-1} were obtained for the MH design. In table 3, we also note that the decay length (defined as the inverse of the argument in the exponential in the force expression) for the force in the Z direction decreases when the stability factor increases suggesting that the increased gradient over compensated for the slightly shorter distance over which the force was applied. As with the previous case the stability factors were found using a 100 nm polystyrene particle as a model target.

Table 3. Trapping stability for a 100 nm diameter polystyrene bead.

Trapping method	Stability factor at 300 K (W^{-1})	Decay length (nm)
Microcavity design (MD)	9 000	60
Mode gap design (MG)	26 000	55
Microcavity plus hole (MH)	44 000	50
Slot waveguides, 65 nm diameter particle [30]	875	50–100

4.2. Particles smaller than the hole diameter

Unlike the previous cases for 100 nm particles, for the MH and MG devices, the most stable position for trapped smaller particles is within the central cavity hole rather than resting on top of the device. The hole walls offer physical confinement in the X and Y directions and thus stiffnesses along these axes are no longer relevant. For these smaller particles, we therefore studied the forces along the Z-axis position while remaining inside the hole. It has already been outlined that for this type of devices [18] the position of a large particle within the hole can affect the resonance. Our simulations confirmed that for a 70 nm polystyrene particle in the central hole of the MH resonator, the resonant wavelength is shifted by 0.4 nm, which is consistent with the results presented by Lin *et al* [18]. For a 40 nm test particle, the resonant wavelength shift was lower than that resolvable by the solution and thus not considered in the simulations. We used a mesh cladding cylinder around the central hole in order to overcome the numerical errors that the shift in the particle's position caused. This 'mesh cladding' served as a shield to the mesh perturbation caused by the changing position of the particle inside the hole.

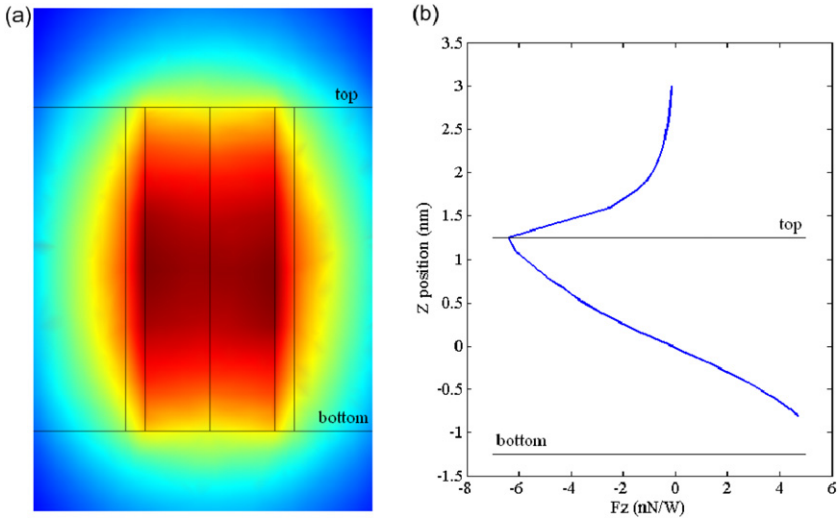

Figure 4. Field and force in the central hole. (a) Representation of E in the central hole in a plane along the resonator. (b) Trapping force in the central hole for a 70 nm polystyrene particle. The Z position represents the position of the centre of the particle. The Z axes in (a) and (b) are not to scale for clarity purposes.

Table 4. Stiffness', and stabilities for smaller particles.

Device	Trapped particle, size (nm)	Trapping stiffness (pN nm^{-1} W^{-1})	Stability (W^{-1})
Microcavity plus hole (MH)	Polystyrene, 70	69	177 000
	Polystyrene, 40	11	70 000
Self-induced back action [21]	Polystyrene, 50	6.6	
Standing Gaussian wave [11]	DVB $n = 1.592$, 50	0.06	

For each position of the particle, we set the wavelength to match the new resonance. As we explain in section 5, the average displacement is small enough that the local variations in the resonant wavelength are negligible. For the 70 nm and 40 nm polystyrene particles, we summarized the calculated stiffnesses and stabilities in table 4. The forces calculation used for the 70 nm case are plotted in figure 4. Because of the enhanced interaction with the field in the hole, the resulting forces are much greater than those for larger particles evanescently trapped. The 11 pN nm^{-1} W^{-1} stiffness we report for a 40 nm particle compares to SIBAs 7.2 pN nm^{-1} W^{-1} for a 50 nm particle [21]. The highest stiffness we report here is that for a 70 nm particle which is 69 pN nm^{-1} W^{-1}. In addition to these stiffnesses, in table 4 we also report the inferred stability number for the SIBA design from the reported trapping energy [21]. Such high figures of merit in both cases are the result of the enhanced field–particle interaction that occurs within the hole in this case, or the hole in the metal sheet for the SIBA design.

5. Discussion

The quest for particle tweezers with higher trapping stiffness and stabilities is justified by the desire to efficiently trap and manipulate smaller molecules and other nanomaterials. In this paper, we explore the possibility of higher stiffness' and forces than what has been previously published. We see from equation (4) that higher trapping stiffness results in better confinement and therefore greater certainty in the particles position. Therefore achieving high trapping stiffness is a necessary step towards handling smaller molecules. For a 100 nm particle and a 10 mW power input, the best design we developed (the MH design) yields the particle's position uncertainty as $\langle x^2\rangle^{1/2} = 4.3$ nm. For the 70 nm and the 40 nm particles, and 10 mW of input power, the particle's position uncertainties are respectively 2.45 nm and 6.1 nm. Over these distances, the resonant wavelength shift is minor. When considering smaller spherical particles, we can use the Rayleigh theory to compute the expected forces, in this case the force varies proportionally to the volume of the particle [12]. With this approach we can derive the following two relations:

$$\left(\frac{D}{40}\right)^{3/2} = \frac{6.1}{\langle x^2\rangle^{1/2}} \tag{6}$$

$$S = 700 \times \left(\frac{D}{40}\right)^{3} \tag{7}$$

where D is the diameter of the Rayleigh particle in nanometres, $\langle x^2\rangle^{1/2}$ and S are the standard deviation on the particle's position and its stability number under a 10 mW of power input. Using the previous relations, we determine the smallest size of a spherical particle allowing for stable trapping ($S > 5$), while having a standard deviation smaller than the hole height ($\langle x^2\rangle^{1/2} < 250$ nm) to be 7.7 nm leading to a stability number of five and a standard deviation of 72 nm. In these cases, the variation in the resonant wavelength due to the random motion

of a trapped particle is expected to be small in comparison with the line width of the resonator and not likely to 'kick' the system out of resonance.

Increasing the trapping parameters is important in order to reduce the power requirements of the trap and by extension the degree of local heating. The most immediate way is through field enhancement (for a constant 1 W of input power). The force is proportional to the number of photons stored in the cavity which is proportional to the Finesse. Therefore a way of increasing the trapping force is building devices with higher Q factors, if the field profile remains similar. One has to be careful when using resonators with higher Q factors as the line width is smaller and the presence of a particle is more likely to kick the resonator out of resonance. This is well known by the biosensing community which uses ultrahigh Q factors to make very precise sensors [16, 31].

Among the exciting possibilities of these devices are those offered by the dependence of the resonant wavelength on the particle's position, in particular it's depth within the cavity hole. With these resonators it is possible to conceive of a power free optical trap by slightly red detuning the excitation from the resonant wavelength when no particle is in the cavity. If properly detuned, when a trapped particle begins to diffuse out of the cavity, it could force the system back into resonance applying a restoring force pushing the particle back into the trap. A particle trapped in the resulting arrangement would not experience any force unless it tries to leave the trap creating an effective optical cage. This leads to a trap with an effective stable volume rather than a stable point. This represents a new type of self-induced trapping mechanism.

6. Conclusion

In this paper, our goal was to illustrate the possibilities offered by integrated optics for the trapping and manipulation of nanoscopic matter. We have evaluated three photonic crystal resonator designs and performed a theoretical study of their specifications as photonic traps. Our calculations indicate an important enhancement of the trapping parameters as compared to the state of the art. In the device offering the best performance, we find stiffness' as high as 22.3 pN nm^{-1} W^{-1} for a 100 nm polystyrene particle, compared with the previously highest reported stiffness of 8.2 pN nm^{-1} W^{-1}. For smaller beads, the field–particle interaction is increased in the central hole leading to increased trapping stiffness's. For a 70 nm particle, we found the stiffness to be 69 pN nm^{-1} W^{-1} to be compared to 6.6 pN nm^{-1} W^{-1} previously reported for 50 nm beads. The confinement in the central hole offers a greatly increased trapping stability with numbers as high as 177 000 W^{-1} for a 70 nm particle and 70 000 for a 40 nm particle. For particles down to 7.7 nm size, we expect 0.08 pN nm^{-1} W^{-1} stiffness and stability as high as 500 W^{-1}. We also highlighted the difficulties and possibilities offered by the use of higher Q factors resonators. Increasing the Q factor increases the forces but also the resonant wavelength shift of the device. It opens some exciting possibilities such as self-induced trapping.

Acknowledgments

This work was supported by the Nanobiotechnology Center (NBTC), an STC Program of the National Science Foundation under Agreement No. ECS-9876771, the National Institutes of Health—National Institute of Biomedical Imaging and Bioengineering (NIH-NIBIB) under grant number R21EB007031 and the US National Science Foundation—CAREER program through grant number 0846489.

References

[1] Ashkin A 1970 Acceleration and trapping of particles by radiation pressure *Phys. Rev. Lett.* **24** 156
[2] Neuman K C and Block S M 2004 Optical trapping *Rev. Sci. Instrum.* **75** 2787–809
[3] Collin D, Ritort F, Jarzynski C, Smith S B, Tinoco I Jr and Bustamante C 2005 Verification of the Crooks fluctuation theorem and recovery of RNA folding free energies *Nature* **437** 231–4
[4] Imasaka T 1998 Optical chromatography. A new tool for separation of particles *Analusis* **26** M53–5
[5] Terray A, Arnold J and Hart S J 2005 Enhanced optical chromatography in a PDMS microfluidic system *Opt. Express* **13** 10406–15
[6] Agarwal R, Ladavac K, Roichman Y, Yu G, Lieber C and Grier D 2005 Manipulation and assembly of nanowires with holographic optical traps *Opt. Express* **13** 8906–12
[7] Jamshidi A, Pauzauskie P J, Schuck P J, Ohta A T, Chiou P Y, Chou J, Yang P and Wu M C 2008 Dynamic manipulation and separation of individual semiconducting and metallic nanowires *Nat. Photon.* **2** 86–9
[8] Greenleaf W J, Woodside M T and Block S M 2007 High-resolution, single-molecule measurements of biomolecular motion *Annu. Rev. Bioph. Biomed.* **36** 171–90
[9] Wang M D, Yin H, Landick R, Gelles J and Block S M 1997 Stretching DNA with optical tweezers *Biophys. J.* **72** 1335–46
[10] Jauffred L, Richardson A C and Oddershede L B 2008 Three-dimensional optical control of individual quantum dots *Nano Lett.* **8** 3376–80
[11] Zemanek P, Jonas A, Sramek L and Liska M 1998 Optical trapping of Rayleigh particles using a Gaussian standing wave *Opt. Commun.* **151** 273–85
[12] Ashkin A, Dziedzic J M, Bjorkholm J E and Chu S 1986 Observation of a single-beam gradient force optical trap for dielectric particles *Opt. Lett.* **11** 288–90
[13] Righini M, Zelenina A S, Girard C and Quidant R 2007 Parallel and selective trapping in a patterned plasmonic landscape *Nat. Phys.* **3** 477–80
[14] Grigorenko A N, Roberts N W, Dickinson M R and Zhang Y 2008 Nanometric optical tweezers based on nanostructured substrates *Nat. Photon.* **2** 365–70
[15] Righini M, Volpe G, Girard C, Petrov D and Quidant R 2008 Surface plasmon optical tweezers: tunable optical manipulation in the femtonewton range *Phys. Rev. Lett.* **100** 186804
[16] Arnold S, Keng D, Shopova S I, Holler S, Zurawsky W and Vollmer F 2009 Whispering gallery mode carousel—a photonic mehanism for enhanced nanoparticle detection in biosensing *Opt. Express* **17** 6230–8
[17] Barth M and Benson O 2006 Manipulation of dielectric particles using photonic crystal cavities *Appl. Phys. Lett.* **89** 253114

[18] Lin S, Hu J, Kimerling L and Crozier K 2009 Design of nanoslotted photonic crystal waveguide cavities for single nanoparticle trapping and detection *Opt. Lett.* **34** 3451–3
[19] Mandal S, Serey X and Erickson D 2010 Nanomanipulation using silicon photonic crystal resonators *Nano Lett.* **10** 99–104
[20] Yang A H J, Moore S D, Schmidt B S, Klug M, Lipson M and Erickson D 2009 Optical manipulation of nanoparticles and biomolecules in sub-wavelength slot waveguides *Nature* **457** 71–5
[21] Juan M L, Gordon R, Pang Y, Eftekhari F and Quidant R 2009 Self-induced back-action optical trapping of dielectric nanoparticles *Nat. Phys.* **5** 915–9
[22] Mandal S, Goddard J and Erickson D 2009 A multiplexed optofluidic biomolecular sensor for low mass detection *Lab Chip* **9** 2924–32
[23] Velha P, Rodier J C, Lalanne P, Hugonin J P, Peyrade D, Picard E, Charvolin T and Hadji E 2006 Ultracompact silicon-on-insulator ridge-waveguide mirrors with high reflectance *Appl. Phys. Lett.* **89** 171121
[24] Jackson J D 1999 *Classical Electrodynamics* 3rd edn (New York: Wiley)
[25] Svoboda K and Block S M 1994 Biological applications of optical forces *Annu. Rev. Biophys. Biomed.* **23** 247–85
[26] Gardiner C W 2004 *Handbook of Stochastic Methods: For Physics, Chemistry, and the Natural Sciences* 3rd edn (New York: Springer)
[27] See for example de Fornel F 2000 *Evanescent Waves: From Newtonian Optics to Atomic Optics* (Berlin: Springer) chapter 3
[28] Rohrbach A 2005 Stiffness of optical traps: quantitative agreement between experiment and electromagnetic theory *Phys. Rev. Lett.* **95** 168102
[29] Zemanek P, Jonas A, Jakl P, Jezek J, Sery M and Liska M 2003 Theoretical comparison of optical traps created by standing wave and single beam *Opt. Commun.* **220** 401–12
[30] Yang A H J, Lerdsuchatawanich T and Erickson D 2009 Forces and transport velocities for a particle in a slotted waveguide *Nano Lett.* **9** 1182–8
[31] Zhu J, Ozdemir S K, Xiao Y-F, Li L, He L, Chen D-R and Yang L 2009 On-chip single nanoparticle detection and sizing by mode splitting in an ultrahigh-Q microresonator *Nat. Photon.* **4** 46–9